SDC-91-00065

SDC
SOLENOIDAL DETECTOR NOTES

SCINTILLATING FIBER DETECTORS

Fiber Tracking Group

SCINTILLATING FIBER DETECTORS*

Fiber Tracking Group (FTG)

B.Abbot[h], D.Adams[i], M.Atac[a,b], C.Anway[a], A.Baumbaugh[b], B.Baumbaugh[d], P.Berge[b], M.Binkley[b], J.Bishop[d], N.Biswas[d], A.D.Bross[b], C.Buchanan[a], N.Cason[d], R.Chaney[j], D.Chrisman[a], A.Clark[b], D.Cline[a], H.Cohn[e], M.Corcoran[i], R.Davies[h], J.Elias[b], E.Fenyves[j], D.Finley[b], G.W.Foster[b], J-M.Gaillard[b], J.Godfrey[d], H.Goldberg[c], H.Hammack[j], X.Huang[d], J.Jaques[d], V.Kenney[d], R.Kephart[b], D.Koltick[h], J.Kolonko[a], K.Kondo[k], R.A.Lewis[g], J.Marchant[d], R.McIlwain[h], S.Margulies[c], H.Miettenen[i], R.Moore[g], R.J.Mountain[d], T.Okusawa[f], J.Piekarz[d], A.Pla-Dalmau[b], R.Ruchti[d], R.Scalise[g], W.Shephard[d], E.Shibata[h], G.A.Smith[g], J. Solomon[c], K.Takikawa[k], S.Tkaczyk[b], and R.Wagner[b]

University of California at Los Angeles[a]
Fermi National Accelerator Laboratory[b]
University of Illinois at Chicago[c]
University of Notre Dame[d]
Oak Ridge National Laboratory[e]
Osaka City University[f]
Pennsylvania State University[g]
Purdue University[h]
Rice University[i]
University of Texas at Dallas[j]
Tsukuba University[k]

Presented by R. Ruchti

INTRODUCTION

The decade of the 1990s will see the construction and commissioning of the Superconducting Super Collider as the one of the World's premier scientific instruments. To meet the challenges of experiment at this new machine, it is essential to have successful development of technologies capable of providing charged-particle tracking and fast triggering on high p_T tracks to the highest luminosities, $L \approx 10^{34}\ cm^{-2}\ sec^{-1}$. Tracking detectors based on scintillating fibers represent one of these important initiatives, particularly for large volume, general-purpose detectors.

The Fiber Tracking Group (FTG) is developing a high-rate tracking subsystem appropriate for SSC applications in general and for the SDC experiment in particular, based on scintillating fiber technology. Typical SSC detector designs contain 10^6 fibers and associated readout channels. Additionally, the group is actively pursuing the development of a 10^5 fiber central tracker for the upgrade of the D0 detector for operation at the Fermilab Main Injector. The use of scintillating fibers as a detection medium affords the prospect for tracking charged particles with high resolution, low occupancy, and very short resolving time, and for providing first-level triggering based on the transverse momentum of charged particles.

PHYSICS CHALLENGE: THE DETECTION OF RARE PROCESSES

An important challenge for any SSC experiment is the provision of an effective tracking detector. Because of the high luminosity environment and the short bunch separation at the SSC, any tracking detector must have fast response, low occupancy, good spatial resolution, and good resistance to radiation damage.

A central tracking system should be capable of reconstructing low-mass states such as the Z^o with a precision of 1-2%, and should enable cross-checks of the electromagnetic and hadronic calorimeter calibration over a wide momentum range. Further, expected topologies such as the Higgs boson, detected via the decay $H \rightarrow Z^oZ^o \rightarrow qqll$ and the decay

*Work Supported by the US Department of Energy, the SSC Laboratory, the Texas National Research Laboratory Commission, and participating Universities and Labs.

$H \rightarrow Z^0 Z^0 \rightarrow$ 4 leptons, should be identifiable, with at least a 3σ charge sign determination for tracks of $p_T \leq 1$ TeV/c.

At an SSC detector operating at machine luminosities $L = 10^{34}$ cm^{-2} sec^{-1}, any viable tracking device must operate reliably in a high radiation environment (typically $< 10^6$ rads in 10 years at a radius r = 60 cm from the interaction region due to beam interactions and neutron albedo). The tracking system, which must have low material thickness, should be capable of reconstructing all tracks, have good rejection against spurious tracks, and should be capable of separating tracks resulting from multiple interactions in a bunch crossing. A number of tracking options are being considered, but so far no technique has been proven. At small radii (typically r < 50 cm) silicon detectors (strips and/or pixels) are being considered for track reconstruction. At larger radii, the possibility of a stand-alone scintillating fiber tracker is potentially very attractive. It should be noted that the advantages of these two detector types are complementary.

Since the first successful use of fiber tracking in a collider environment [1], significant progress has been made [2]. Fiber trackers have the following attractive features.

1. Good tracking precision: multilayer structures of 750μm diameter fibers can result in a measurement resolution of 60μm per layer [3,4] and provide good two track resolution.

2. Fine granularity: for fibers of 750μm diameter and 4m length placed at radii r = 60cm, the worst case occupancy from all sources is expected to be < 3.2% (< 21%) per fiber, per bunch crossing, at a luminosity $L = 10^{33}$ (10^{34}) cm^{-2} sec^{-1}. [5] For fibers placed at larger radii, the occupancies are substantially lower.

3. Good time resolution: an intrinsically prompt response;

4. Insensitivity to magnetic fields and to RF noise;

5. Simple electronics: binary (yes/no) readout is used;

6. No power dissipation in the tracking volume; and

7. The possibility to develop a level 1 trigger based on transverse momentum of individual charged particle tracks [4,6,7].

However, several technological developments are required before a realistic scintillating fiber central tracker for SSC detectors can be claimed. Figure 1 shows a hypothetical central tracking system [8] which covers the kinematic range $|\eta| \leq 2.5$. For $|\eta| \leq 1.6$ the geometry is cylindrical. Tracking in this region is accomplished with four superlayers, each comprised of four sublayers of fibers of 750μm diameter and lengths ≤ 4m. Two of these sublayers contain axial fibers (x) which measure rφ coordinate, and two provide narrow angle stereo (u,v) measurements (refer to Figure 2). As shown in Figure 3, the placement of component fiber layers within a sublayer can be adjusted to provide optimal spatial resolution. Four layers of fibers of 750μm diameter each offset by 1/4 of a diameter, lead to a position resolution of 60μm per sublayer[3]. Because of the flexibility of the fibers, stereo layers can be wrapped in a helical fashion, and different stereo angles can be chosen for each superlayer to avoid ghosts in pattern recognition. Typical choices are angles in the 4°-10° range, with larger stereo angles at smaller radii to improve the resolution in longitudinal coordinate. For the intermediate region $1.6 \leq |\eta| \leq 2.5$, the flexibility and field immunity of scintillating fibers permits novel arrangements of detection elements. Figure 4 shows one possibility in which sublayers of spiral right and left coordinates are combined with a sublayer of fibers positioned azimuthally [8]. With this particular configuration, development of a fast trigger on stiff

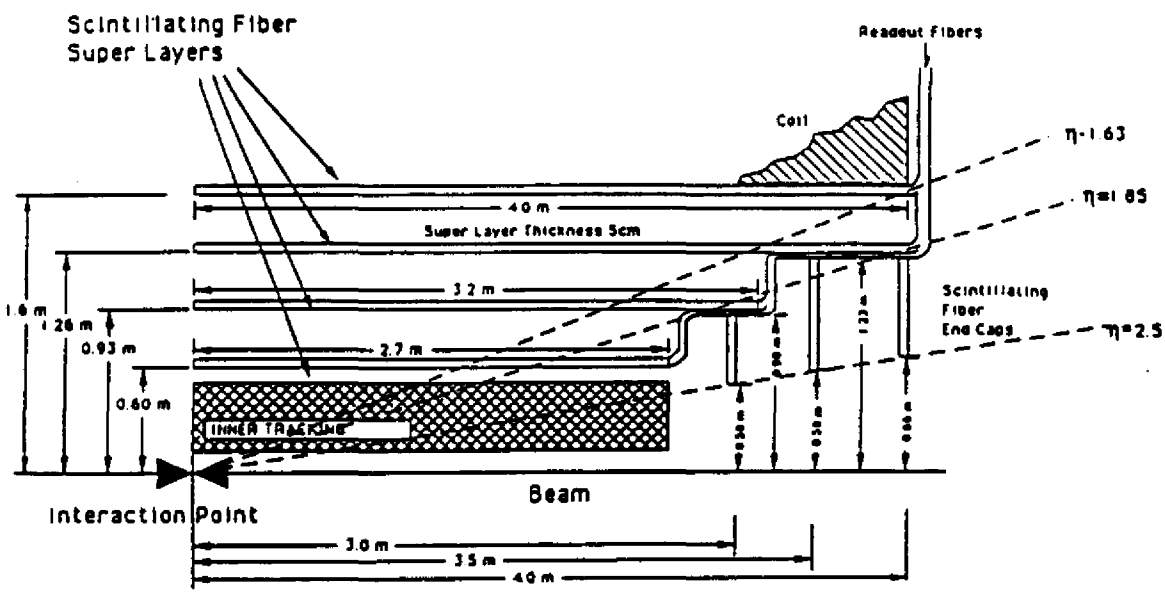

Figure 1. Schematic of a central tracker based on scintillating fibers.

tracks is straightforward, through the use of look up tables.

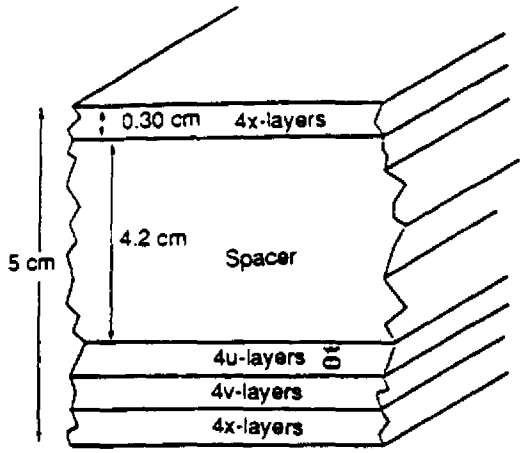

Figure 2. Schematic of a Scintillating Fiber Superlayer

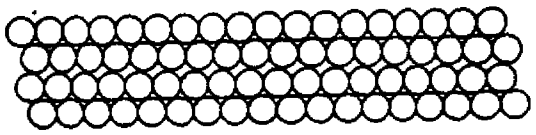

Figure 3. Placement of component fiber layers within a sublayer for optimal spatial resolution. The effective spacing of the layers is 1/4 of a diameter, by shifting the lower doublet relative to the upper doublet.

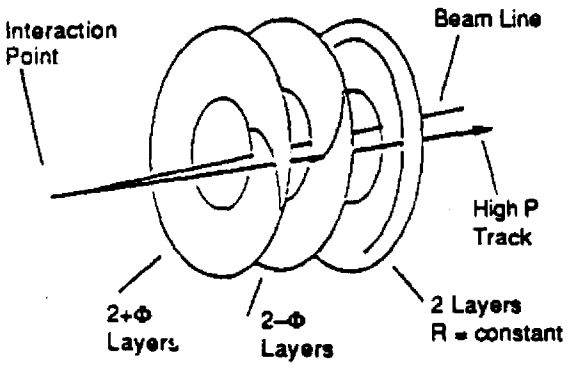

Figure 4. Possible fiber superlayer structures for intermediate tracking, $1.6 < |\eta| < 2.5$.

For the fiber tracker, the basic detection element is an active scintillator fiber of ≤ 4m length, coupled via a 4m-5m long, clear fiber waveguide to a high-rate photodetector. The performance goals are: the detection of minimum ionizing particles resulting from a beam-beam collision with an efficiency exceeding 95% per layer; the determination of the longitudinal coordinate and impact parameter to 1mm for each track; unambiguous assignment of each track to a beam crossing (16 nsec time interval); momentum resolution sufficient to reconstruct the mass of the Z^0 to < 2% in a leptonic decay; momentum resolution sufficient to make a 3σ determination of the charge of a 1 TeV/c particle; and radiation resistance adequate for all components to survive for several years of beam without significant degradation of capabilities.

EXPERIMENTAL CHALLENGE: THE DETECTION OF SCINTILLATION LIGHT

The challenge of scintillating fiber tracking is the efficient and effective detection of scintillation photons created by minimum ionizing particles in a large volume detector. A schematic of a fiber tracking element is shown in Figure 5. It includes: a scintillating fiber; a "clear" fiber-optic waveguide which is optically coupled (spliced) to the scintillating fiber; and optical coupling of the waveguide fiber to a photodetector. Of these, the scintillating fiber is the active detection element. The clear fiber waveguide acts as a convenient means of propagating the scintillation information to the location of a photodetector whose position may be remote (typically several meters) from the actual detector region.

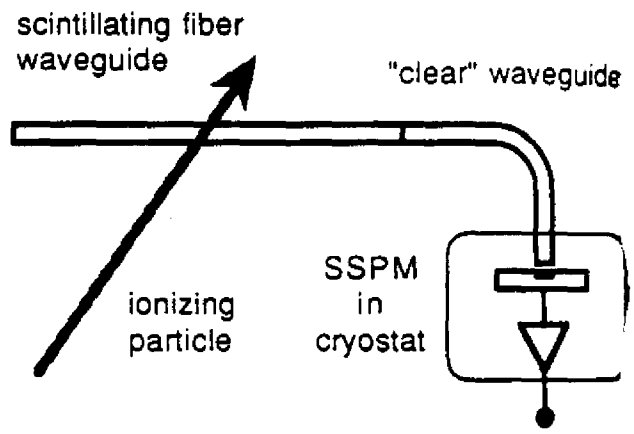

Figure 5. Schematic of a single fiber tracker channel.

The nature of the photodetection problem is indicated numerically in the Equations 1-3 below [9,10,11]:

$$I(z_s+z_w) = I_o\, F\, A(z_s,z_w)\, G_{pm}\, Q_{pm} \quad (1)$$

with:

$$I_o = (dE/dx)\, \Delta x_{eff}\, V_{eff}\, (Q_{sc}/\Delta E_{eff})\, C_{uv} \quad (2)$$

and:

$$A(z_s,z_w) = \exp(-z_s/\Lambda_s)\, T_1 \exp(-z_w/\Lambda_w)\, T_2 \quad (3)$$

where:

$I(z_s+z_w)$ is the detected number of photoelectrons detected at the photodetector located at a total distance z_s+z_w from the scintillation site, where z_s is the effective path length in scintillation fiber material and z_w is the effective path length in the waveguide fiber material.

I_o is the average yield of scintillation photons produced by a minimum ionizing particle in the scintillating fiber, and averaged over the effective cross sectional area of the fiber.

The various quantities which contribute to I_o include:

dE/dx the mean energy loss per unit length.
Δx_{eff} is the effective path length of scintillator through which the particle passes.
V_{eff} is the fraction of the fiber volume occupied by the core, hence active scintillation material.
Q_{sc} is the quantum efficiency of the scintillator.
ΔE_{eff} is the effective deposited energy to generate a scintillation photon, ($\Delta E_{eff} \sim 1239.8/\lambda(nm)$ in eV).
Λ_{uv} is the mean free path for waveshifting between primary and secondary dyes.
C_{uv} is the efficiency of UV light conversion between primary and secondary dyes.

F is the fraction of light emitted from the secondary dye (i.e. the resultant scintillation light) which is trapped by total internal reflection in the fiber waveguide material [9].

$A(z_s,z_w)$ is the overall attenuation factor for light propagating in the waveguide from the scintillation site to the photodetector. It includes separate exponential terms for attenuation in the scintillation and waveguide fibers which depend in part on the reflection coefficients between core and cladding and in part on optical absorption. The attenuation lengths Λ_s and the glass capillary and plastic fiber cool, the plastic, having greater thermal contraction, pulls away from the glass wall, allowing it to be withdrawn. may themselves be functions of path length, in which case the attenuation is not a single exponential. Additionally, there are two transmission coefficients: T_1 is the optical transmission at the splice between scintillator and waveguide fibers; and T_2 is the optical transmission through the cryostat boundary.

G_{pm} is the the geometric efficiency for light collection at the photodetector.

Q_{pm} is the quantum efficiency of the photodetector.

A summary of numerical values for these paramaters are given in Table I for a 1mm diameter scintillating fiber composed of polystyrene and the dyes PTP and 3HF. Where possible, measured values are listed. Otherwise the parameter values have been calculated or estimated from Monte Carlo simulation.

Photoelectron Yield

Inserting these values into Equation 1, and assuming fiber scintillators and waveguides each of 4 meter length, $z_s = z_w =$ 4m, we expect to detect an average of $I(z_s+z_w) = I(4+4) = 4.5$ photoelectrons from such a fiber tracking element of 1mm diameter using currently available fiber technology. For 750μm diameter fibers, we expect ≥ 3 photoelectrons. While these yields represent a major achievement already, they are marginal for a large scale system. For implementation in an SSC central tracker composed of 10^6 fiber elements as discussed above, it is desireable to have a safety margin of a factor of ~ 2 in light yield, recognizing that additional light losses will be incurred when an actual detector is constructed. We now discuss the key issues involved, to achieve this goal.

Table I. Values of parameters used in Equations 1 - 3.

Parameter	Value	Status	Ref.
dE/dx	2 MeV/cm	Meas	
Δx_{eff} (norm. inc)	0.78mm	Calc	
V_{eff}	0.94	Calc	
Qsc	0.04	Meas	[nuc]
ΔE_{eff}	4.77eV	Meas	[16]
Λ_{uv}	1.3mm	Calc	
C_{uv}	0.7	Calc	[Fig.7]
F (min,max)	0.031,0.048	Calc	[9]
Λ_s	6m	Meas	[10]
Λ_w	10m	Meas	[14,15]
T_1	0.95	Meas	[18]
T_2	0.9	Est	
G_{pm}	0.96	Calc	[Fig.11]
Q_{pm}(min)	0.6	Meas	[19]

Values are based on a 1mm diameter scintillating fiber. The fiber is assumed to be composed of a polystyrene core of 970μm diameter containing PTP and 3HF primary and secondary dyes. The cladding wall is assumed to be 15μm thick PMMA. The status column indicates whether the value is measured, calculated, or estimated.

Discussion of Fiber Detector Characteristics

For a scintillating fiber tracking element to provide high detection efficiency, hence $I(z_s+z_w)$ large, the following requirements must be satisfied:

1. The effective quantum efficiency of the active fiber element must be high, with local light emission within the fiber. As shown in Table II taken from references [12,13], a number of new promising candidate scintillation materials have been developed. Many of these have fluorescence efficiency which exceeds that of standard scintillators such as polystyrene/PTP/DMPOPOP. Even more impressive is the combination of high efficiency with long wavelength fluorescence, a feature which is essential for good optical

transmission in polystyrene as indicated in Figure 6 [1,14,15]. Attenuation lengths in excess of $\Lambda_s \geq 5$m are desireable.

Table II. Light output before and after 10 Mrad radiation dose from a ^{60}Co source in arbitrary units.

Scintillator[a]	λ[b] (nm)	Light output Before	After	After 13 d[c]
MOPOM	420	0.79	.04	.42
MOPOM+.01%BBQ	470	0.95	.13	.63
MOPOM+.02%BBQ	470	0.96	.16	.69
MOPOM+.01%K27	500	0.95	.27	.75
MOPOM+.02%K27	500	0.95	.27	.75
O415A	415	0.92	.49	.79
O415A+.01%BBQ	470	1.01	.42	.86
O415A+.02%BBQ	470	1.02	.34	.89
O415A+.01%K27	500	0.97	.57	.87
O415A+.02%K27	500	0.99	.53	.88
O408	410	0.88	.48	.76
O408+.02%BBQ	470	1.02	.34	.87
O408+.02%K27	500	0.97	.57	.89
DAT	375	0.73	.16	.46
DAT+DMPOPOP	430	0.86	.31	.70
DAT+.01%3HF	530	0.85	.40	.63
pT	360	0.84	.21	.41
pT+DMPOPOP	430	0.88		

[a]Fluor concentrations are by weight, the concentrations of primaries are 1% (1.25% for DAT).[b]Wavelength of peak emission. [c]Annealed 10 days in oxygen and 3 days in air.

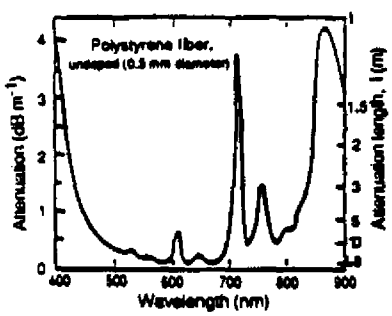

Figure 6. Optical attenuation in 500μm clear polystyrene waveguide as a function of wavelength [1,14,15].

There are several important contributions to this high efficiency. First is the energy level overlap between primary dye and the solvent polystyrene. As indicated in the references [12,13], the efficiency reaches a maximum when the primary concentration is 1% by weight in the material as expected from a non-radiative energy transfer mechanism (Forster Transfer) between the solvent and primary [16,17]. Second is energy overlap between the primary and secondary dyes, for efficient waveshifting (following Beer's Law)[16]. The efficiency of this waveshift is a function of the fiber waveguide material (here assumed to be a polystyrene core with acrylic cladding) and the mean-free-path Λ_{uv} of photons emitted by the primary and absorbed by the secondary. Numerically, Λ_{uv} is inversely proportional to the product of the molar concentration and wavelength-dependent, molar extinction coefficient of the secondary dye. The fiber efficiency is displayed as a function of Λ_{uv} in Figure 7 based on a Monte Carlo simulation program discussed in reference [9], assuming a uniform distribution of dyes in the fiber. For a standard scintillator in which DMPOPOP is the secondary, Λ_{uv}~200μm. Hence ~92% of the light would be effectively waveshifted in a 1mm diameter scintillating fiber of this material, hence C_{uv}=0.92 [18]. By contrast, the mean-free-path for a fiber incorporating 3HF as the secondary is Λ_{uv}~1300μm, which leads to C_{uv}=0.70. Note that there is a minimum of efficiency C_{uv}~0.55, which is determined by total internal reflection of light at the cladding/air interface, i.e. the exterior wall of the fiber. (This minimum efficiency level may well be influenced (lowered) through uv absorption by the polystyrene particularly in the presence of radiation damage.)

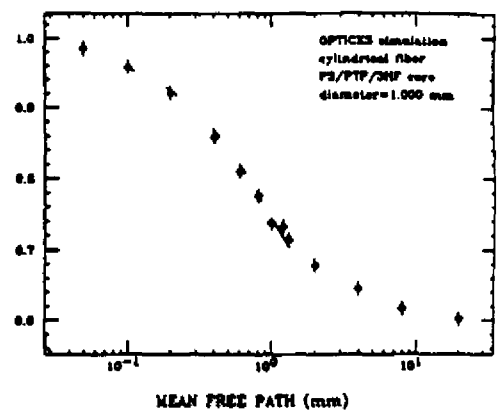

Figure 7. Fiber Efficiency (C_{uv}) as a function of Λ_{uv} (See text)

2. In general the fluorescence decay time of a scintillator is usually determined by the secondary dye and should be as fast as possible. Under SSC conditions, this would require return to baseline in a time of order 16ns. Scintillators containing secondaries such as K27, BBQ, and their variants have fluorescence decay times in the range $10 \leq \tau \leq 12$ ns, whicle others such as G1 and 3HF are in the $3 \leq \tau \leq 6$ ns range.

3. The chemical properties of the scintillator should be selected so that the material is radiation-resistant and has good optical transparency to the produced scintillation light (i.e. low self-absorption). Radiation resistance in polystyrene based scintillators depends, in part, upon emission wavelength. As

shown in Figure 8, the optical transparency of bulk polystrene has a marked cutoff at a wavelength $\lambda \sim 500$ nm for an applied dose of 10 Mrad of ^{60}Co gamma radiation. The expected integrated radiation dose from all sources for an inner fiber superlayer at r = 60cm is expected to be ~ 1 Mrad in 10 years of operation at luminosities $L = 10^{34}\ cm^{-2}\ sec^{-1}$, based on calculations using information from the LBL Report on Radiation Damage [19]. As indicated in Table I, many of the newly developed scintillation materials have the potential to survive in such a hostile environment, but additional radiation damage measurements will be performed to confirm this.

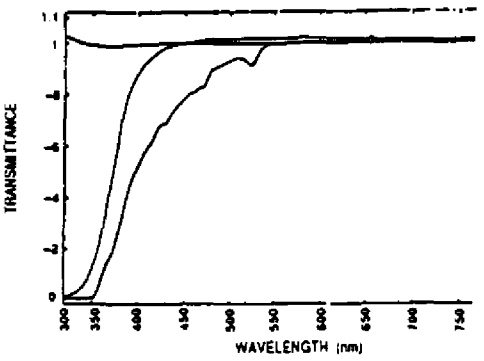

Figure 8. Optical transmission in undoped polystyrene as a function of wavelength, prior to irradiation (upper), immediately after irradiation (lower), and after annealing (intermediate).

4. The mechanical properties of the scintillating fiber materials and the effects of the fiber drawing process must be optimized so that a high reflection coefficient (R ~ 1) can be maintained at the interface between the core and cladding of the fiber waveguide. The characteristics of this interface become yet more important as the ratio of refractive indices of the core and cladding is increased. As discussed in reference [9], the fraction of scintillation light trapped by total internal reflection (F in Equation 1) depends sensitively on this ratio, since a larger ratio of refractive indices implies a larger critical angle. Increasing the critical angle means more boundary encounters (internal reflections) per unit distance along the fiber. Hence higher reflection coefficients R are required to realize a net increase in overall detected light yield.

To date, our studies have been focussed principally on fibers with polystyrene cores and acrylic (PMMA) claddings, because of the considerable experience in drawing such materials by private industry. Refractive indices of the core and clad are n=1.59, n=1.49 repectively at λ=580nm, and the cladding wall thickness is typically 15μm for a 1mm diameter fiber. It should be noted that there are a number of important new initiatives in the area of core and cladding for fibers, particularly low index claddings, and these are being pursued.

5. Optical splicing between scintillation and waveguide fibers should be physically robust and provide a very high transmission coefficient ($T_1 > 0.95$, where T_1 is the coupling coefficient utilized in Equation (3) above). Splicing of scintillation fibers to waveguide fibers has been accomplished by a thermal fusion method [20]. Highly reproducible, robust splices have been produced by this method, with typical optical transmission in excess of 95% integrated over all wavelengths of interest (see Figure 9).

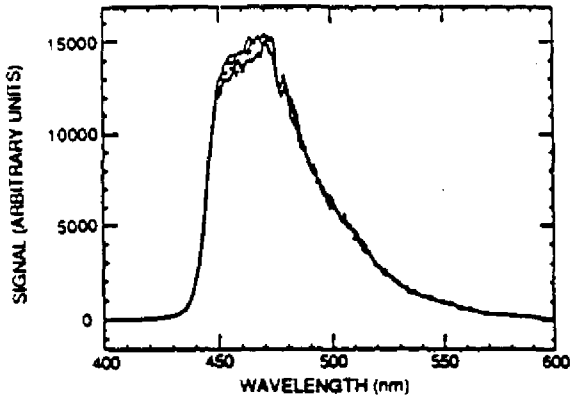

Figure 9. Optical transmission as a function of wavelength for spliced fibers. Solid Lines indicate measurements on the near (detector) side of the splice, dotted lines indicate measurements on the far side of the splice.

6. Clear (non-scintillating) optical fiber waveguides should have long attenuation length for scintillation light ($\Lambda_w \sim 10$m). As discussed in Sections 1 and 3 above and illustrated in Figure 6, such transmission is possible in clear polystrene at wavelengths in the visible region of the optical spectrum, $480 \leq \lambda \leq 700$nm, and depends critically on the purity of the materials used to make the core and cladding, as well as the mechanical preparation of preforms and the quality of the fiber drawing.

7. Coupling of the waveguide fiber to the photodetector must be straightforward. For devices which operate at room temperature such as phototubes, this poses no problem. For cryogenically operated solid-state photodetectors such as Solid State Photomultipliers (SSPMs) [21,22] and Visible Light Photon Counters (VLPCs) [23], this requires extra care in the design and maintenance of cryogenics, the fiber-optic link between ambient temperature and the cryogenic environment in which the photodetectors reside, and mechanical infrastructure. Polystyrene fibers, both scintillating and non-scintillating, have been found to provide reliable optical interconnection between room temperature and 7K where the SSPMs and VLPCs operate efficiently. Such fibers have been cycled many times between these temperature extremes without mechanical failure in laboratory tests.

An assessment of the coupling efficiency between fiber waveguide and photodetector, T_2 in Equation (3) above, has been provided by waveguide simulation [9]. Figure 10 shows light rays emergent from the end of a scintillating fiber of 500μm diameter, having polystyrene core and acrylic cladding, assuming uniform illumination by scintillation light over the

cross sectional area of the fiber, generated several meters from the end of the fiber. Figure 11 shows the fraction of emergent rays from a 1mm diameter fiber which strike a photodetector facing the end of the fiber, as a function of separation distance between fiber and detector, and for various detector sizes. As long as the photodetector is positioned within 1/4 diameter from the end of the fiber, geometric efficiency is excellent (G_{pm}~96%) and crosstalk to adjacent photodetector elements is minimal.

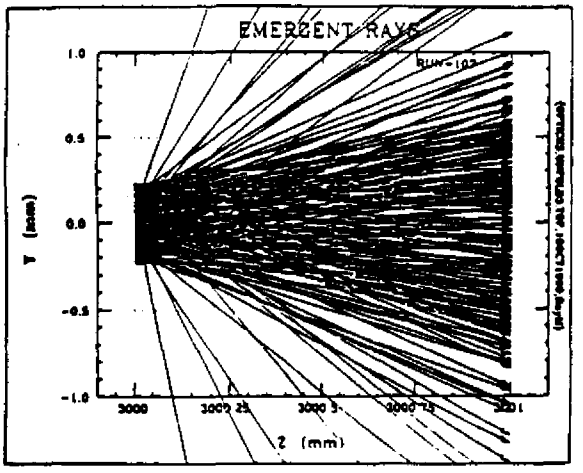

Figure 10. Monte Carlo simulation of light rays emerger from the end of a fiber scintillator of polystyrene core and PMMA cladding.

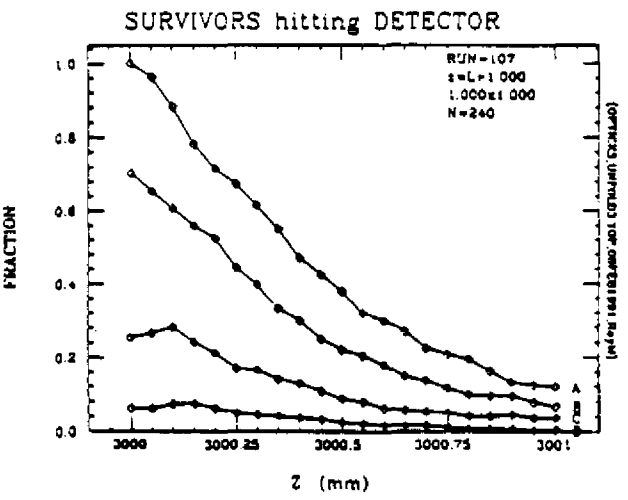

Figure 11. Fraction of light emergent from a fiber waveguide, detected by an VLPC/SSPM as a function of geometry.

8. It is essential that the quantum efficiency of the photodetector be as high as possible at the wavelengths of interest (Q_{pm}> 50%) and, additionally, that the photodetector have fast response. The Solid State Photomultilplier (SSPM) developed by Rockwell [21] incorporates both of these features. Figure 12 shows a schematic of the SSPM. A variant of this structure, VLPC, which is sensitive to visible light only, is under contractual development with Rockwell International Science Center as part of the FTG Subsystem program for SSC applications. As shown in Figure 13, the quantum efficiency of the SSPM structure is Q_{pm}~60% at all visible wavelengths λ>400nm. For the VLPC structure, Q_{pm} is expected to reach 80%. These values are to be contrasted with typical quantum efficiencies of photomultiplier tubes utilizing bialkali or multialkali transmission photocathodes which are at least a order of magnitude lower at wavelengths λ>530nm.

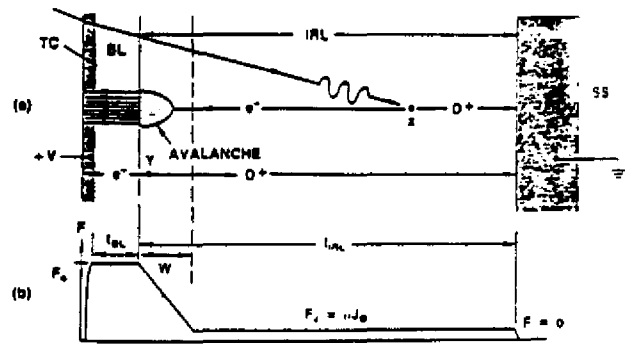

(a) SSPM LAYER CONFIGURATION WITH SCHEMATIC REPRESENTATION OF THE GENERATION OF BIAS CURRENT AND THE EFFECTS FOLLOWING ABSORPTION OF A PHOTON.
(b) ELECTRIC-FIELD PROFILE

Figure 12. Schematic of the SSPM device.

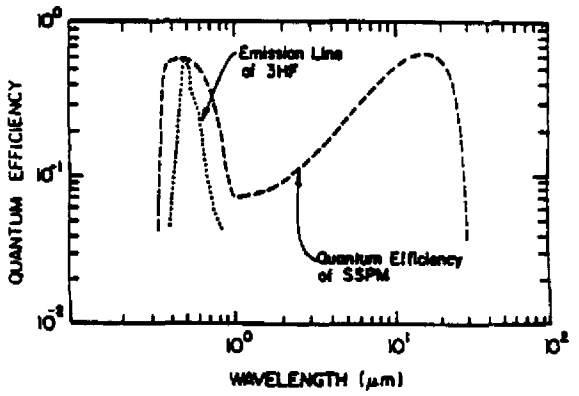

Figure 13. Quantum Efficiency of the SSPM as a function of wavelength.

For operation with high gain, good gain dispersion, and good signal to noise characteristics, the SSPM must be cryogenically cooled to ~7K. Typical gain is 5×10^4, and as shown in Figure 14, the device is a marvelous single photon counter. Peaks corresponding to 1-10 simultaneously detected

photoelectrons are easily recognizable in these distributions [23]. Such spectra are obtained routinely when light yields are measured for scintillating fibers which fluoresce at wavelengths in the visible region, and illustrate graphically the capability of the SSPM, and its significance for fiber tracking.

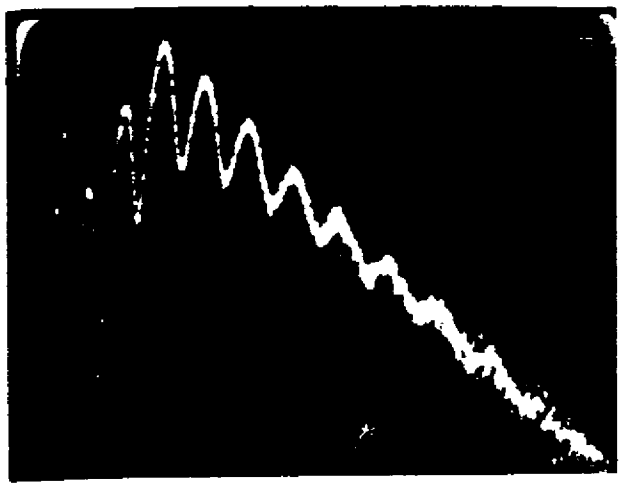

Figure 14. Spectrum of simultaneously detected photoelectrons observed using an SSPM to detect light from a 500μm diameter scintillating fiber with emission at 530nm. Up to 10 distinct photo- electron peaks are discernable. Vertical scale is logarithmic.

An additional important feature of the SSPM/VLPC structure is that devices can be prepared as discrete detectors or in linear arrays and mosaics of detection elements of arbitrary size and complexity. For SSC applications, a linear array of detector elements has been selected as the architecture for initial development [23]. A number of preamplifier options are under consideration for use with the VLPC/SSPM devices, some of which operate cryogenically [24].

Cryogenic heat loads for SSPM/VLPC operation have been estimated [25]. A tracking system of 10^6 scintillating fibers, each coupled to its own VLPC channel, cryogenically cooled preamp, driver and signal cable, constitutes a 150W load for a helium refrigeration system, under high luminosity conditions ($L = 10^{34}$ cm^{-2} sec^{-1}). This is to be compared to a Tevatron ring magnet which requires ~10W of refrigeration.

9. Lastly, the key components of a fiber tracking elements: fiber scintillator, fiber wavguide, photodetector, and ancillary readout electronics must be studied for radiation sensitivity. Important sources of damage are gamma, charged particle and neutron fluences. Such measurements are planned during the next year. However it should be noted that the photodetection elements will be situated outside of the calorimetry where radiation levels are expected to be low.

Improvements to Detected Photoelectron Yield

Possible improvements in overall photoelectron det. efficiency are summarized in Table 3. These include impr quantum efficiency of the VLPC devices, improved scintillation materials and fiber manufacture, and careful study and implementation of new cladding materials. While it is unlikely that each of the listed benefits will be realized in full measure, nevertheless it is expected that a combination of these will lead to sufficient improvement that an overall factor of two in detected photoelectrons can be realized..

Table III. Potential Improvements to Detected Photoelectron Yield

Item	Factor
Improved QE of VLPC over SSPM	1.4
Improvement in dye C_{uv}	1.3
Improvement in fiber manufacture	1.5
Improvement in light trapping using low refractive index claddings. (Must be accompanied by simultaneous improvement in reflection coefficient in order to be realized.)	1.5 - 3

TRACKING SYSTEM PERFORMANCE

Online Implementation

As discussed in above, the strengths of a fiber tracker are its intrinsic speed and high granularity. These features are being exploited in the development of a Level 1 trigger capability. The principal requirement at this level is to identify charged particle trajectories with a minimum transverse momentum $p_T \geq 10$ GeV/c. Such a trigger must correctly identify high p_T tracks from interesting physics processes, while having excellent rejection power against fake high p_T tracks created by chance correlations (pileup) of minimum bias events.

One possible trigger scheme is: first to select a hit in the tracking superlayer at largest radial distance from the interaction point, then pick a second hit at the intermediate tracking layer affording the maximum sagitta, and finally search for hits in other layers as a redundancy check. This procedure has been studied in simulation [7]. Figure 15 shows the probability per beam crossing for detecting a fake high p_T track based on fiber tracking information only. At a luminosity of 10^{33}, requiring the participation of 3/4 of the tracking elements in the identification of a trajectory leads to a probability of triggering on a fake high p_T track at the level; at higher luminosity, 10^{34}, one must require

available tracking elements to achieve a probability of 10^{-1}. [26] Such identified trajectories can be simultaneously associated with deposited energy in calorimetry towers, again at the timing of Level 1, leading to powerful discrimination for electrons at the earliest stages of the trigger chain.

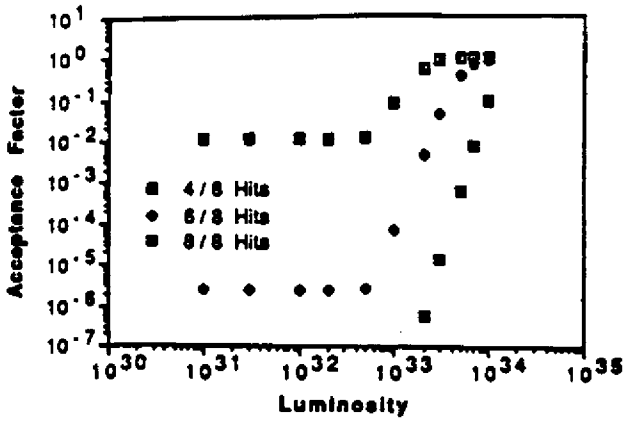

Figure 15. Simulated acceptance for fake tracks in a 650μm scintillating fiber tracker. Vertical scale is probability per beam crossing.

As discussed in references [4,6], a level 1 hardware trigger architecture is being developed which provides rapid determination of the sagitta of a particle track. Initial prototyping is based on discrete technology, whereas ultimate implementation will incorporate ASIC technology. The technique involves identifying clusters of hits in fiber sublayers, then correlating pairs of sublayer clusters within a superlayer, and finally connecting track segments between superlayers. Figure 16 taken from reference [4] indicates schematically the appearance of a low momentum track and a high Pt track, as they would appear in the two sublayers which form a superlayer. The illustrated condition is 3% occupancy.

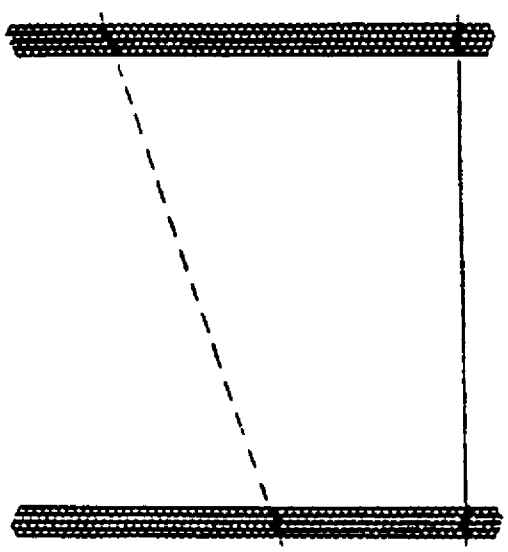

Figure 16. Scintillating fiber superlayer with a radial track (solid line) and a low momentum track (dashed line). Occupancy is 3%. Clusters are shown in the sublayers.

Functionally, the trigger starts from the outer superlaye and linking proceeds toward the origin, assuming a bea constraint. The search road for a 10 GeV/c track is high restrictive, since the sagitta for such a trajectory is 2cm over radial distance of 1.6m. Reconstructed tracks and associat quality factors (whether found in three or four superlayers) a then sent to trigger decision logic. For a track, the azimuth coordinate is partly encoded by the physical cable and partly b data. The momentum is encoded as the sagitta in units of fib diameter. The resolution in momentum is better than 0.004p at the trigger level, and will be implemented with pipeline AND/OR logic. Figure 17 shows a schematic of the trigg architecture.

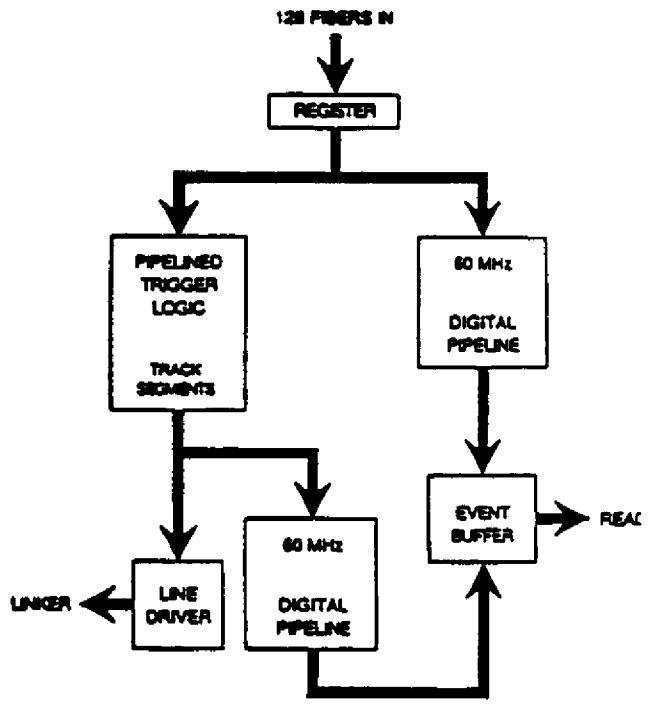

Figure 17. Functional block diagram for digital AS combining pipeline delay with track segment finding the trigger.

Offline Implementation

A substantial effort is underway to develop a detai simulation and analysis code for fiber tracking based GEANT [5,27]. Momentum resolution for central trackin found to be excellent - particularly when incorporating a ver constraint or tracking information from a vertex or microver tracking system. The expected performance for the rapic interval $|\eta|<1.6$ is: $dp_T/p_T \sim 0.2p_T$ (TeV/c) with no be constraint, and $dp_T/p_T \sim 0.1p_T$ (TeV/c) with beam constr [28].

CONCLUSIONS

Scintillating Fibers can provide a powerful means for tracking charged particles in SSC experiments. Substantial Research and Development work still remains, particularly in the areas of scintillation materials and waveguides, and the incorporation and interfacing of these structures with solid state photodetectors. A subsystem program is being carried out by the Fiber Tracking Group directed at these important issues, and substantive beam tests are planned as part of this program, beginning early in 1991 at Fermilab.

REFERENCES

[1] J. Allitti, et al, IEEE Transactions on Nuclear Science, Vol. 36, No. 1(1989) 29-34.

[2] For a comprehensive review of the field and recent progress see: The Proceedings of the Workshop on Scintillating Fiber Detectors for the SSC, Fermilab, November 14-16, 1988, S. Reucroft and R. Ruchti, eds., and various contributions by FTG to these proceedings.

[3] This intrinsic positional accuracy is determined from $750\mu m/(4\sqrt{12})$ which is $55\mu m$. When combined in quadrature with a fiber placement/alignment accuracy of $25\mu m$, the overall measurement resolution is expected to be of order $60\mu m$.

[4] J. Elias, et al, these proceedings.

[5] D. Adams, et al, these proceedings.

[6] G.W. Foster, et al, these proceedings.

[7] R. A. Lewis, et al, these proceedings.

[8] The hypothetical tracker shown is one of the prototypical designs under consideration for the Solenoid Detector Collaboration (SDC). See also D. Koltick, et al, these proceedings.

[9] R.J. Mountain, et al, these proceedings.

[10] B. W. Baumbaugh, et al, paper submitted to the Proceedings of the 1990 IEEE Nuclear Science Symposium, Crystal City, VA, October 1990.

[11] R. Ruchti, lectures on Scintillating Fiber Detectors at the ICFA Summer School on Instrumentation in Particle Physics, Rio de Janeiro, July, 1990.

[12] J. Pickarz, et al, these proceedings.

[13] A. Pla--Dalmau, et al, paper submitted to the Proceedings of the 1990 IEEE Nuclear Science Symposium, Crystal City, VA, October, 1990.

[14] C. Hurlbut, Bicron Corporation, private communication.

[15] T. Kaino, M. Fujiki and K. Jinguji, Review of the Electrical Communication Laboratories, Vol. 32, No. 3, (1984) 478-488.

[16] I. Berlman, *Handbook of Fluorescence Spectra of Aromatic Molecules*, Academic Press (1971).

[17] J. B. Birks, *Theory and Practice of Scintillation Counting*, Pergamon Press (1964).

[18] In the UA2 experience, little improvement was found when the scintillating fibers used for this experiemt were aluminized, in an effort to trap more UV light within the fiber. Figure 7 illustrates that the improvement could be at most 8-10%, consistent with their observations. However, it should be noted that significant improvement (>30%) could be expected for fibers containing secondary dyes such as 3HF, which are in low concentration and/or have low molar extinction coefficients.

[19] D. Groom, et al, Radiation Levels in SSC Interaction Regions, SSC-SR-1033 (1988).

[20] M. Atac, G. W. Foster, and M. Lundun, "A Simple Method for Fusing Plastic Fibers", Fermilab Technical Note FN-537, March, 1990.

[21] M. D. Petroff and M. G. Stapelbroek, IEEE Transactions on Nuclear Science, Vol. 36, No.1, (1989) 158-162.

[22] M. D. Petroff and M. Atac , IEEE Transactions on Nuclear Science, Vol. 36, No.1, (1989) 163-164.

[23] M. Atac, et al, these proceedings.

[24] R. Chaney, et al, these proceedings.

[25] S. Margulies, et al, these proceedings.

[26] As indicated in reference 7, this performance is superior to other large-volume tracking alternatives such as straw tube detectors.

[27] C. Anway, et al, these proceedings.

[28] A summary of system resolution is provided in the Expression of Interest to the SSC Laboratory by the Solenoidal Detector Collaboration, 24 May, 1990, and in the subsequent Letter of Intent.